Rapid source characterization of the 2011 M_w 9.0 off the Pacific coast of Tohoku Earthquake

Gavin P. Hayes[1,2]

[1]*U.S. Geological Survey, National Earthquake Information Center, Golden, CO, USA*
[2]*Synergetics Inc., Fort Collins, CO, USA*

(Received April 8, 2011; Revised May 12, 2011; Accepted May 15, 2011; Online published September 27, 2011)

On March 11th, 2011, a moment magnitude 9.0 earthquake struck off the coast of northeast Honshu, Japan, generating what may well turn out to be the most costly natural disaster ever. In the hours following the event, the U.S. Geological Survey National Earthquake Information Center led a rapid response to characterize the earthquake in terms of its location, size, faulting source, shaking and slip distributions, and population exposure, in order to place the disaster in a framework necessary for timely humanitarian response. As part of this effort, fast finite-fault inversions using globally distributed body- and surface-wave data were used to estimate the slip distribution of the earthquake rupture. Models generated within 7 hours of the earthquake origin time indicated that the event ruptured a fault up to 300 km long, roughly centered on the earthquake hypocenter, and involved peak slips of 20 m or more. Updates since this preliminary solution improve the details of this inversion solution and thus our understanding of the rupture process. However, significant observations such as the up-dip nature of rupture propagation and the along-strike length of faulting did not significantly change, demonstrating the usefulness of rapid source characterization for understanding the first order characteristics of major earthquakes.
Key words: Great earthquake, earthquake rupture processes, 2011 off the Pacific coast of Tohoku Earthquake, source inversion.

1. Introduction

Current estimates indicate that the moment magnitude M_w 9.0 off the Pacific coast of Tohoku Earthquake of 2011-03-11 (hereafter the Tohoku Earthquake) is likely to be the most costly natural disaster ever in terms of economic losses resulting from the earthquake and its subsequent tsunami (Risk Management Solutions, http://bloom.bg/jlAxHl); preliminary estimates suggest losses of 200–300 billion US dollars. In stark contrast to these figures and the accompanying devastation and loss of life, this earthquake is also likely to be the best-recorded event of its kind, in terms of data density and diversity both regionally in Japan, and globally at seismic stations across the world. These data sets will hopefully spawn research related to earthquake engineering, the earthquake rupture, tsunami generation, the aftershock sequence, and other observations of the seismic cycle in unprecedented detail. While such studies will ultimately provide the most complete picture of the event, it is also important and informative to explore the rapid analyses of the earthquake—what we knew when, and how much this information evolved over the following days and weeks.

To that end, we describe here the source characterization of the Tohoku Earthquake performed as part of real-time response efforts at the U.S. Geological Survey (USGS) National Earthquake Information Center (NEIC). We focus on the specifics of this rapid source inversion and its updates, rather than on other aspects of the earthquake, such as how this event fits in to our seismologic and tectonic understanding of the Japan Trench; these issues are covered well by others and do not need to be repeated here.

The NEIC is federally mandated to determine the location and size of all significant earthquakes worldwide, and to immediately disseminate this information to concerned national and international agencies, scientists, critical facility operators, and the general public. A key part of this response is the characterization of the earthquake source through rapid finite-fault estimates of earthquake slip distributions. For the Tohoku event, these provided accurate estimates of slip extent within seven hours of the earthquake origin time (Hayes *et al.*, 2011). While these early estimates have been, and will continue to be, surpassed by many subsequent detailed and less time-sensitive analyses (including our own updates to the initial model), the semi-automated and real-time aspects of this work are unique. Inherent trade-offs therefore exist between speed and accuracy of such solutions, and these issues will be discussed. We also show how such uncertainties can be reduced by the consideration and incorporation of a priori information on fault geometry (in this case, using the USGS Slab1.0 model, http://on.doi.gov/d9ARbS; Hayes *et al.*, 2009a) as constraints on the fast finite fault inversion. Finally, we briefly discuss the broad range of downstream products and models that utilized this rapid source characterization.

doi:10.5047/eps.2011.05.012

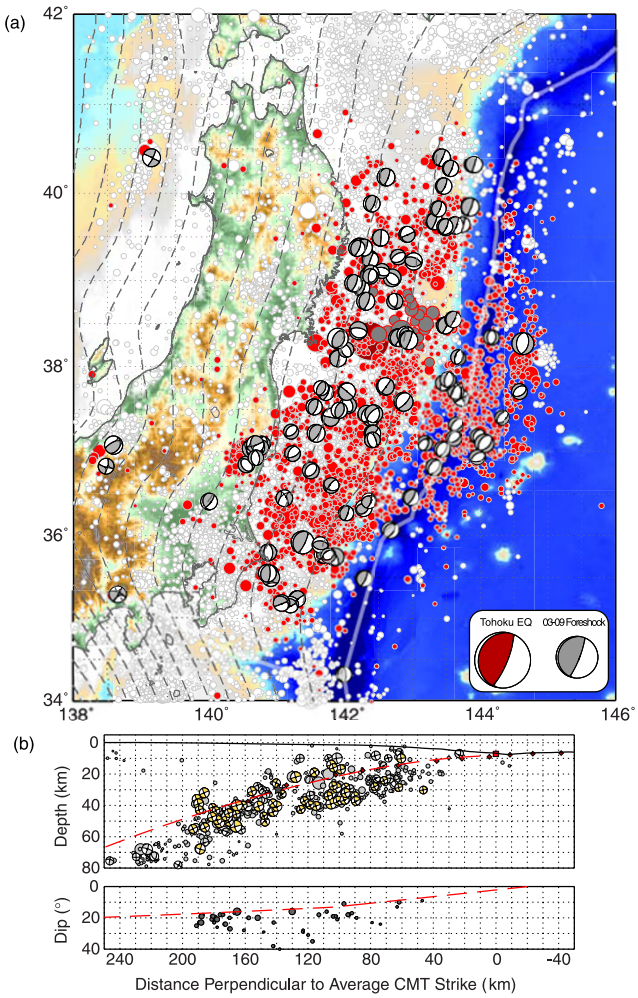

Fig. 1. Map of the tectonic setting of the March 2011 Tohoku Earthquake. The large maroon circle is the USGS NEIC epicenter of the mainshock; red dots with gray outlines are aftershocks, through the end of April 2011. White circles with gray outlines represent seismicity prior to March 9th 2011. Dark gray circles with red outlines represent foreshocks of the Tohoku event, beginning with the M_w 7.3 March 9th earthquake. All circles have radii scaled according to each earthquakes magnitude. Light gray focal mechanisms are gCMT (http://www.globalcmt.org) solutions of aftershocks, plotted at the equivalent USGS NEIC locations. Dark gray dashed lines represent the depth of the subducting Pacific slab, from Slab1.0 (http://www.earthquake.usgs.gov/research/data/slab), in 20 km intervals. The thick transparent white line represents the major plate boundary. Inset shows the USGS W-phase CMT solutions for the mainshock and 03/09 foreshock. Part (b) shows a cross-section of the subduction zone through the hypocenter of the mainshock (gray star), overlain with a 2D profile through Slab1.0. Yellow CMTs are gCMT solutions used to constrain the slab geometry; gray circles represent background seismicity. Red diamonds represent data from local active seismic surveys, also used to constrain geometry. See URL (above) for more details. The lower panel shows the dip of the Slab1.0 interface.

2. The Tohoku Earthquake

On March 11 2011, at 05:46:23 UTC (14:46 at the epicenter) a great M_w 9.0 earthquake struck offshore of northeast Honshu, Japan (epicentral location 38.322°N, 142.369°E, depth 32 km; USGS NEIC, http://on.doi.gov/jkjnap). The earthquake ruptured a section of the Japan Trench (marking the interface between the overriding North America plate and subducting lithosphere of the Pacific plate) just ~300 km long and ~150 km wide, with peak slips of 35 m or more. The relatively condensed, shallow rupture spawned a large tsunami that devastated the coastline of eastern Honshu (Y. Okada, Preliminary report of the 2011 off the Pacific coast of Tohoku Earthquake, http://bit.ly/lVKMwA). The event was a surprise to many, occurring in a subduction zone that had not witnessed an event larger than M_w 8.2 throughout Japan's long historic records (Tanioka *et al.*, 1997).

The USGS W-phase (Kanamori and Rivera, 2008; Hayes *et al.*, 2009b; Duputel *et al.*, 2011a, b) centroid moment tensor (CMT) solution (http://on.doi.gov/hiuizE) shows the earthquake ruptured a shallow thrust fault that aligns well with the geometry of the Japan Trench (Fig. 1), with a best double-couple fault plane of strike $\varphi = 195°$, dip $\delta = 14°$, and rake $\lambda = 87°$. This solution has a seismic moment of $m_o = 3.85 \times 10^{29}$ dyne-cm. The global CMT (gCMT; http://www.globalcmt.org) solution has a seismic moment of $m_o = 5.31 \times 10^{29}$ dyne-cm, 38% higher than the W-phase solution, which may be a result of the lower dip of the gCMT shallow nodal plane ($\delta = 10°$), and the well-known trade-off between seismic moment and dip for shallow earthquakes (Kanamori and Given, 1981). In either case, these solutions indicate that this earthquake represents the fourth-largest event recorded during the modern era of instrumental seismology.

3. Preliminary Finite Fault Inversion

The NEIC uses a finite fault inversion approach based on the method of Ji *et al.* (2002). The procedure inverts both body-wave (*P* & *SH*, band-pass filtered between 1–200 s) and surface wave (Rayleigh and Love, band-pass filtered between 200–500 s) data on a planar fault surface generally aligned with early estimates from CMT solutions. Data are chosen based on producing an azimuthally balanced data set, while avoiding the inclusion of data with small signal-to-noise ratios. Rupture velocity can be fixed or allowed to vary; generally for rapid response efforts we allow a broad distribution of velocities to account for unknown rupture characteristics. We also test both nodal planes of the initial CMT solution to account for the uncertainty over which describes the causative fault. Initial fault length is estimated from empirical relations between duration and moment (Dahlen and Tromp, 1998), scaled to length assuming a rupture velocity of 2.5 km/s, and doubled to account for uncertainty in rupture direction (i.e., centered bilaterally on the hypocenter). Fault planes are divided into a series of subfaults along the strike and dip directions, and we invert for the slip amplitude, direction, rise-time and rupture initiation time of each subfault, where subfault source time functions are modeled with an asymmetric cosine function (Ji *et al.*, 2002, 2003). The model is referenced spatially to the preliminary USGS NEIC hypocenter; uncertainty in this location likely affects peak slip estimates

For the Tohoku Earthquake, our first, automated estimates of slip distributions (approximately 1.75 hours after the earthquake origin time) used data from 40 globally distributed stations, with 40 *P*-waves, 20 *SH*-waves, and 60 long period surface waves each 200 s in length. Fault geometry followed an early USGS W-phase solution (strike $\varphi = 162°$, dip $\delta = 17°$; Duputel *et al.*, 2011b), with subfaults

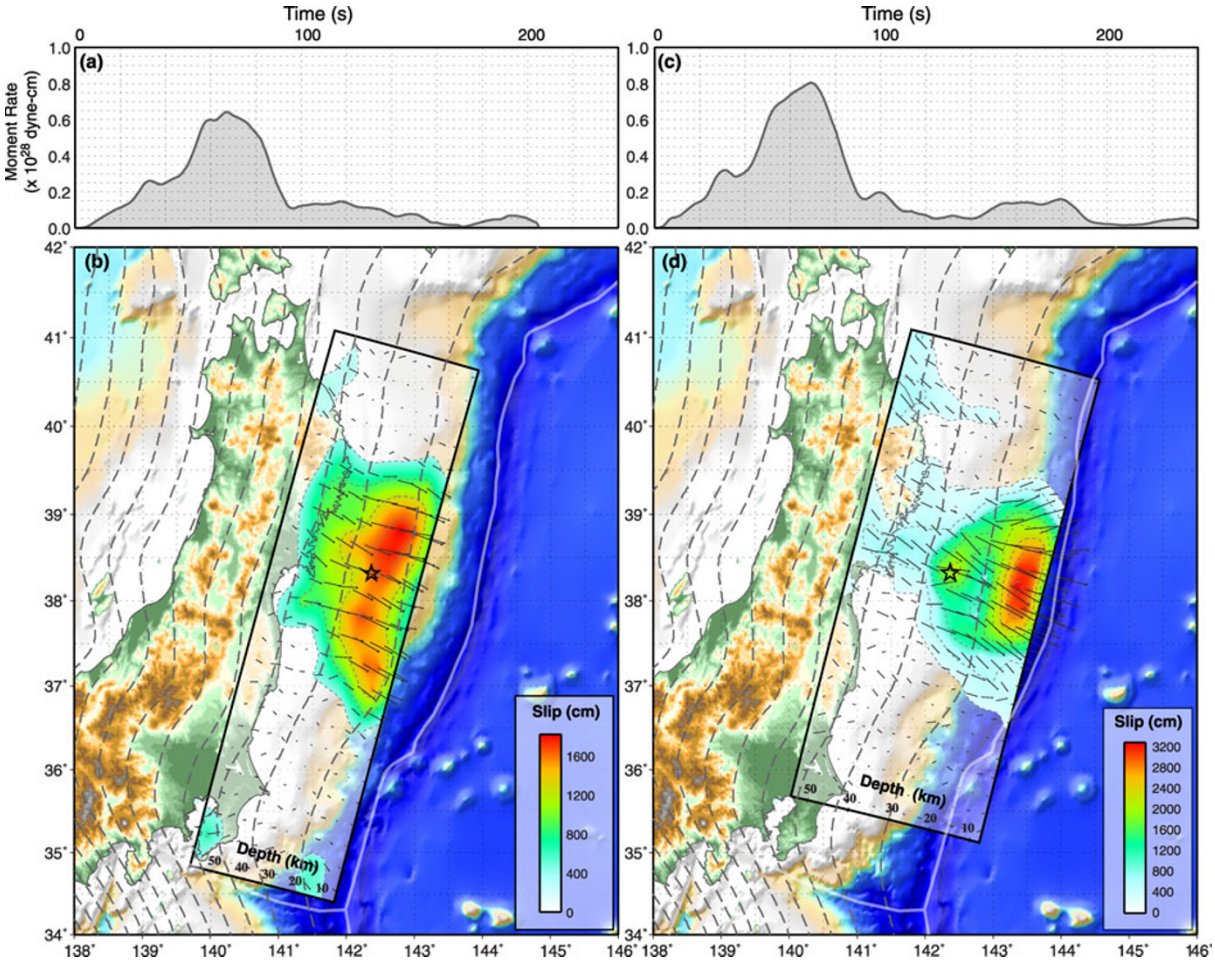

Fig. 2. Maps of the initial (a, b) and updated (c, d) USGS NEIC finite fault slip distributions of the Tohoku Earthquake. Panels (a) and (c) show source time functions of each solution. In each map panel (b) and (d), the inverted slip distribution is shown within the assumed rectangular fault geometry, colored by slip magnitude, and contoured every 4 m. Regions with slip below 4 m are partially transparent. The slip vector of each subfault is represented with a black arrow, also scaled by slip magnitude.

30 km in length along strike, and 20 km in width along the dip-direction of the fault. The preliminary USGS hypocenter location was used (Lon. 142.37, Lat. 38.32, Dep. 25 km) as the nucleation point of the rupture. The solution suffered from misaligned fault geometry with respect to slab structure, and from difficulties in the parameterization of rupture velocity and peak slip. Specifically, the source time function of the earthquake (http://on.doi.gov/jymeMM) indicates a relatively emergent start to the event, and thus the position of first significant moment release is poorly constrained; thus even moderate rupture velocity forces delayed moment release away from the hypocenter, if subfault slip durations are not extended to compensate. Similarly, computation times of inversions can be sped up if peak slips are constrained in an automated sense by historic observations. For the Tohoku Earthquake, peak slips were larger than expected based on modeled slip in past large events.

These issues were corrected by using *a-priori* fault strike information from the Slab1.0 global subduction interface model (Hayes *et al*., 2009a; Fig. 1) and by allowing a broader range of rupture velocities and slip in the inversion procedure, resulting in our preliminary model, which provided the first accurate estimate of the distribution of slip on the Japan Trench subduction zone (Fig. 2(b)). This model has a seismic moment of $m_o = 4.04 \times 10^{29}$ dyne-cm (M_w 9.00), peak slips of approximately 18 m, and explains over 91% of the waveform data (measured via least-square error between data and synthetics). The model was available and distributed internally and externally within 7 hours of OT, and was posted on NEIC event pages several hours later. While the model has since been updated (see http://on.doi.gov/h32IYb; Fig. 2(d)) to better account for subduction zone dip, data distribution and quality, the general along-strike and up-dip distribution of slip estimated by this first model is very similar to those shown in a variety of models released since that time.

The updated solution differs from the initial solution in several key ways. First, the geometry of the fault was again adjusted to match the approximate average dip of the subducting interface (using Slab1.0) over the shallow region of the local subduction zone, up-dip of the hypocenter (where the majority of slip occurs in the preliminary model). This gives a dip of $\delta \sim 10^\circ$. The top of the fault was constrained to coincide with the depth of the Japan Trench updip of the hypocenter, approximately 7 km. The depth of the earthquake was also moved from 25 km to 30 km, accounting for updated USGS broadband depth estimates, and aligning more closely with slab depth at the epicenter. Subfault

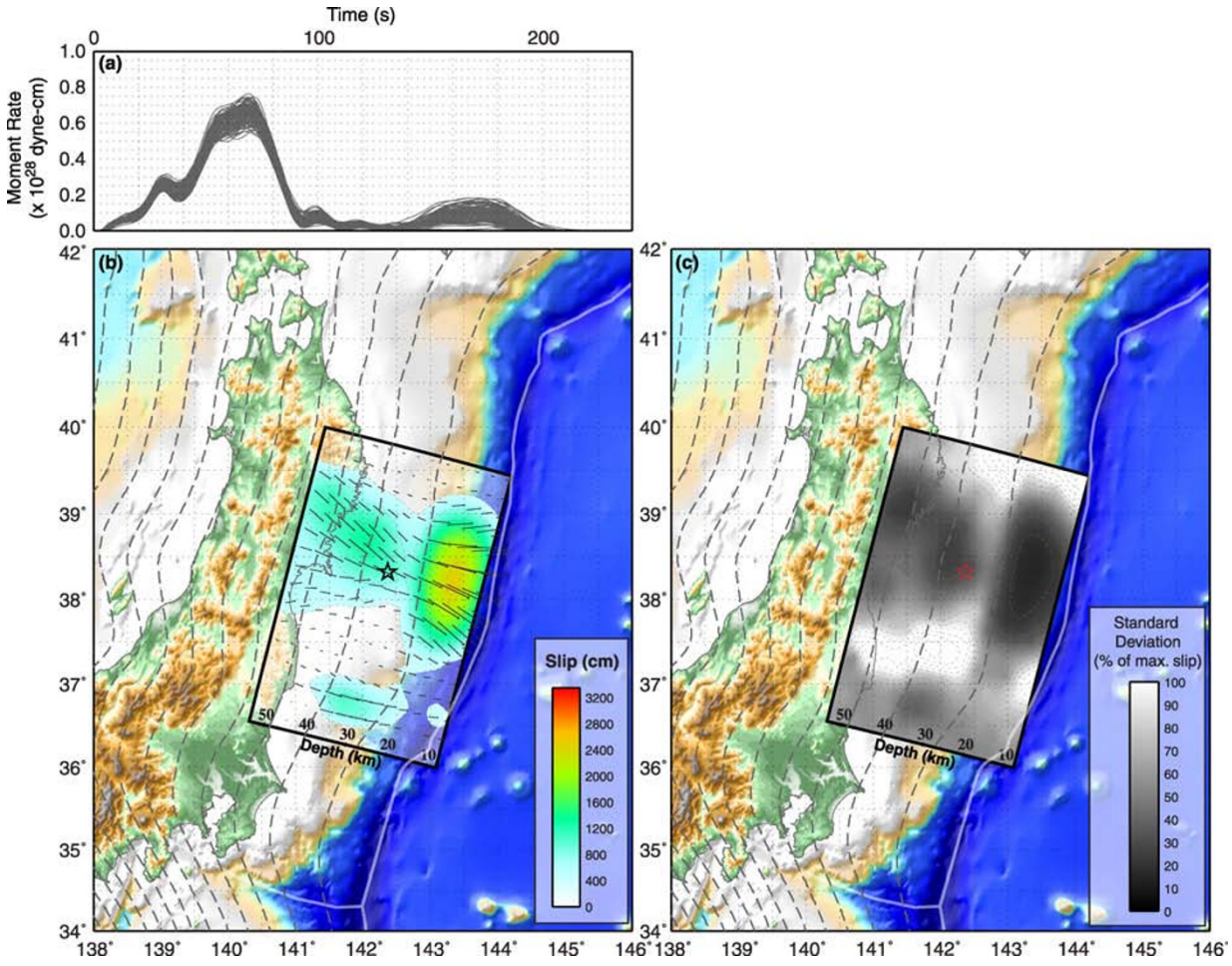

Fig. 3. Map of a bootstrapped, averaged slip distribution. Figure properties follow those of Fig. 2. Panel (a) shows the source time function of each bootstrap solution. In (b), we show the average slip distribution of all 116 inversions. The starting model is the updated USGS NEIC model from Fig. 2(d). In (c), we show the standard deviation of each subfault as a percentage of subfault slip from the average model (SD%), to quantify the resolution of the inversion. Where SD% is low, we expect higher resolution.

lengths were slightly reduced, to 25 km along strike. The data set was adjusted slightly to use a selection of stations more evenly distributed azimuthally, while removing poor quality waveforms. Each subfault was allowed to rupture for a longer period of time (rise time up to 30 s). Rupture velocity and maximum slip were left relatively unconstrained (V_r = 1.25–3.25 km/s; maximum slip = 100 m), and moment minimization constraints were reduced, such that moment is controlled by the inverted data rather than by an assumed initial condition. This model has a seismic moment of $m_o = 4.90 \times 10^{29}$ dyne-cm (M_w 9.06), peak slips over 32 m, and explains over 92% of the waveform data (Fig. 2(d)), and was released approximately 3 days after the earthquake. While such data misfits are difficult to compare given the changes to the input data, this model is preferred based on its better match to source fault geometry and the reduced constraint to inversion input parameters.

In both models, source time functions (Fig. 2(a, c)) show significant moment release lasting approximately 140–150 s, with an emergent start and a steady increase over the first 40 s, and major moment release episodes occurring at approximately 40 s and 70 s. After this second episode, moment release falls off rapidly to a lower level after 100 s. Both models also show late moment release after 140 s, though this appears unconstrained spatially and is restricted to the edges of the fault in both cases. Spatially, slip occurs predominantly up-dip of the hypocenter, towards the trench. In the updated model, slips reach ~15 m close to the hypocenter and peak levels of ~34 m in the 10–16 km depth range. The slip distribution is bilateral and spatially concentrated, extending approximately 125 km to the north and south of the hypocenter. Major slip (>25 m) occurs over one patch roughly 125 × 40 km in size (5 × 2 subfaults).

4. Resolution Tests of Slip Inversions

To explore how well constrained are some of the broad features of our model, we conduct two basic tests. First, we explore the effects of rupture velocity by performing several inversions with fixed V_r, over a range from 1.0–3.0 km/s. For each individual inversion, subfault length (L_x) is adjusted such that the term L_x/V_r is constant. Second, we analyze the spatial resolution of slip with respect to input data by performing a bootstrap analysis (with variable V_r), in which we randomly select 116 'new' data from the 116 input data, and reinvert. This resampling is repeated 116 times, and an average is taken of the resulting models (Fig. 3).

Rupture velocity model tests show that both peak slip and slip location (slip depth) are dependent on V_r; peak slip reaches ~55 m for the lowest rupture velocities, and ~35 m for the fastest. The best-fitting solution is with V_r = 2.5 km/s, though all models explain the data at the 90% level or higher. All models demonstrate up-dip rupture, indicating that the shallow nature of long period energy release is well constrained. Once rupture velocities reach 2.0 km/s, peak slips reach the top layers of the model, and expand bilaterally along the shallowest subfaults as rupture velocities increase further. Rupture lengths vary from ~150 km with V_r = 1.0 km/s, to ~300 km with V_r = 3.0 km/s.

Bootstrap analysis of the USGS updated solution (Fig. 2(d)) show striking similarity in source time functions and slip distributions for the first ~140 s of the earthquake rupture (Fig. 3(a)), and significantly more variability beyond this time, indicating the position and size of late moment release is poorly constrained by these data and inversion approach. In the central portion of the fault, moment release appears very similar to the major features of the updated model, though with lower peak slip (~25 m), and broader slip down-dip of the hypocenter. This model has a seismic moment of $m_o = 3.44 \times 10^{29}$ dyne-cm (M_w 8.96). The reduction in peak slip and inverted moment are likely an artifact of the averaging of many models with variable rupture velocity, and thus with slip distributions that differ slightly spatially.

In an attempt to quantify the resolution across the fault plane using this inversion approach, we compute the standard deviation of slip in each subfault, over all 116 models, normalized by the slip in each cell (%SD; Fig. 3(c)). General features of this display appear similar to Fig. 3(b), though it is clear that the southern edge of the model has lower resolution than the central portion, with standard deviations 60% or more of inverted slip values (i.e. low slip, high standard deviation, vs. <20% near the hypocenter, indicating high slip, low standard deviation). We note that high %SD in the central portion of the fault where slip is near zero is a result of consistent low slip in the bootstrapped models, rather than low resolution in this region. The indication of low resolution at the southern end of the model indicates that late moment release is poorly constrained, and is unlikely to occur at the edges of the inverted fault plane shown here. More detailed analyses of both seismic and GPS data sets may help to constrain the absolute location of this moment release, potentially using finite fault inversions techniques that permit re-rupturing of subfaults after the initial slip pulse has passed (e.g., Lay *et al*., 2010).

5. Discussion

As part of the USGS NEIC real time response to the great March 11, 2011 Tohoku Earthquake, teleseismic body- and surface-wave data were used to rapidly constrain the space-time history of the rupture process. This approach produced a slip model within 7 hours of the origin time of the earthquake. Though this preliminary model was later adjusted for fault geometry better aligned with the subducting Pacific slab, and for less restrictive inversion assumptions, general features of the slip distributions such as the up-dip nature of moment release and the along strike, bilateral rupture length are very similar. This demonstrates the broad applicability of fast finite fault inversions for other aspects of rapid event characterization, such as estimates of spatial shaking distributions, tsunami modeling, and static stress transfer calculations. The initial NEIC finite-fault model was in fact used in the hours following its release for several analyses, including for USGS ShakeMap (http://on.doi.gov/5vpuDw), for stress transfer/triggering modeling (http://on.doi.gov/lD2SAF), and for tsunami simulation (http://on.doi.gov/myzpRH).

Uncertainty in the nodal planes of early moment tensor estimates speak to the usefulness of using a priori information, such as from models like Slab1.0, to constrain initial fault geometries. Here, the use of this model earlier could have reduced the time to the first published slip distribution by as much as two thirds, by eliminating early iterations of the inversion that adjusted fault geometry.

Basic resolution tests show that the depth and along-strike distribution of moment release are dependent on the rupture velocity used in the inversion procedure. A constant rupture velocity of V_r = 2.5 km/s matches data best in comparison to other models with fixed V_r, while a model with variable V_r over a range from 1.25–3.25 km/s performs better still. All models show that rupture velocity was likely variable and relatively slow, with V_r < 2.75 km/s. Tests also show that the up-dip nature of moment release, and the features of the first ~140 s of slip are well constrained by our inversion approach, providing a reliable characterization of the bulk features of the Tohoku Earthquake rupture process.

Acknowledgments. This manuscript benefited from careful reviews by Victor Tsai, David Wald, and two anonymous reviewers—I thank each of them for their insightful comments. The basis of this effort forms part of the broader response by the NEIC, USGS, and other agencies, to the Tohoku Earthquake, and I thank everyone involved in that response for their tireless work on March 11 and beyond. Rapid fault inversions at the NEIC would not be possible without the work of Chen Ji at the University of California Santa Barbara; I thank him for his effort and support. Data used for realtime analyses discussed here are predominantly from the IRIS/USGS Global Seismic Network. Figures in this manuscript were made using the Generic Mapping Tools software package (Wessel and Smith, 1998).

References

Dahlen, F. A. and J. Tromp, *Theoretical Global Seismology*, Princeton University Press, Princeton, NJ, 1998.

Duputel, Z., L. Rivera, H. Kanamori, and G. Hayes, W-phase fast source inversion for moderate to large earthquakes (Mw>=6.5, 1990 - 2010), *Geophys. J. Int*., 2011a (submitted).

Duputel, Z., L. Rivera, H. Kanamori, G. P. Hayes, B. Hirshorn, and S. Weinstein, Real-time W phase inversion during the 2011 off the Pacific coast of Tohoku Earthquake, *Earth Planets Space*, **63**, this issue, 535–539, 2011b.

Hayes, G. P., D. J. Wald, and K. Keranen, Advancing techniques to constrain the geometry of the seismic rupture plane on subduction interfaces a priori: Higher-order functional fits, *Geochem. Geophys. Geosyst*., **10**, doi:10.1029/2009GC002633, 2009a.

Hayes, G. P., L. Rivera, and H. Kanamori, Source inversion of the W-phase: realtime implementation and extension to low magnitudes, *Seismol. Res. Lett*., **80**, 817–822, doi:810.1785/gssrl.1780.1785.1817, 2009b.

Hayes, G. P., P. S. Earle, H. M. Benz, D. J. Wald, R. Briggs, and the

USGS/NEIC Earthquake Response Team, 88 hours: the U.S. Geological Survey National Earthquake Information Center response to the March 11, 2011 Mw 9.0 Tohoku earthquake, *Seismol. Res. Lett.*, 2011 (accepted).

Ji, C., D. J. Wald, and D. V. Helmberger, Source description of the 1999 Hector Mine, California, earthquake, part I: wavelet domain inversion theory and resolution analysis, *Bull. Seismol. Soc. Am.*, **92**, 1192–1207, 2002.

Ji, C., D. V. Helmberger, D. J. Wald, and K.-F. Ma, Slip history and dynamic implications of the 1999 Chi-Chi, Taiwan, earthquake, *J. Geophys. Res.*, **108**, doi:10.1029/2002JB001764, 2003.

Kanamori, H. and J. W. Given, Use of long-period surface waves for rapid determination of earthquake source parameters, *Phys. Earth Planet. Inter.*, **27**, 8–31, doi:10.1016/0031-9201(81)90083-2, 1981.

Kanamori, H. and L. Rivera, Source inversion of W phase: speeding up seismic tsunami warning, *Geophys. J. Int.*, **175**, 222–238, 2008.

Lay, T., C. J. Ammon, A. R. Hutko, and H. Kanamori, Effects of kinematic constraints on teleseismic finite-source rupture inversions: Great Peruvian earthquakes of 23 June 2001 and 15 August 2007, *Bull. Seismol. Soc. Am.*, **100**, 969–994, doi:10.1785/0120090274, 2010.

Tanioka, Y., L. Ruff, and K. Satake, What controls the lateral variation of large earthquake occurrence along the Japan Trench, *The Island Arc*, **6**, 261–266, 1997.

G. P. Hayes (e-mail: ghayes@usgs.gov)